Inorganic Chemistry

pubs.acs.org/IC Article

Butyltin Keggin Ion with a Rare Four-Coordinate Ca Center

Danielle C. Hutchison, Rebecca D. Stern, Lev N. Zakharov, Kristin A. Persson, and May Nyman*

Cite This: Inorg. Chem. 2020, 59, 2900−2909

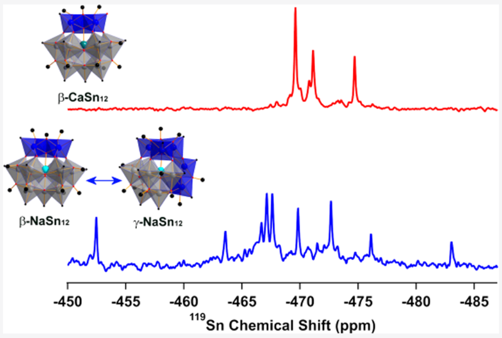

ABSTRACT: Alkyltin clusters are exploited in nanolithography for the fabrication of microelectronics. The alkyltin Keggin family is unique among Keggin clusters across the periodic table; its members appear to favor the lower-symmetry β and γ isomers rather than the highly symmetrical α and ε isomers. Therefore, the alkyltin Keggin family may provide important fundamental information about the formation and isomerization of Keggin clusters. We have synthesized and structurally characterized a new butyltin Keggin cluster with a tetrahedral Ca^{2+} center, fully formulated $[(BuSn)_{12}(CaO_4)(OCH_3)_{12}(O)_4(OH)_8]^{2+}$ (β-$CaSn_{12}$). The synthesis is a simple one-step process. Extensive solution characterization including electrospray ionization mass spectrometry, small-angle X-ray scattering, and multinuclear (^1H, ^{13}C, and ^{119}Sn) nuclear magnetic resonance shows β-$CaSn_{12}$ is essentially phase-pure and stable. This differs from the previously reported Na-centered analogues that always form a mixture of β and γ isomers, with facile interconversion. Therefore, this study has clarified prior confusion over complex spectroscopic and crystallographic characterization of the Na-centered analogues. Density functional theory calculations showed the following stability order: γ-$CaSn_{12}$ < γ-$NaSn_{12}$ < β-$CaSn_{12}$ < β-$NaSn_{12}$. The β analogue is always more stable than the γ analogue, consistent with experiment. Notable outcomes of this study include a rare tetrahedral Ca coordination, a Na-free alkyltin cluster (important for microelectronics manufacturing), and a better understanding of Keggin families built of different metal cations.

INTRODUCTION

The Keggin ion is an important structure in inorganic chemistry, which consists of a central tetrahedral $\{MO_4\}$ unit surrounded by 12 metal-oxo octahedra arranged into four trimers. This structure is formed from metals across the periodic table, including W, Mo, Nb, Fe, Al, Cr, Sb, and Sn.[1−9] There are five rotational isomers of the Keggin ion,[10] denoted by the Greek letters α, β, γ, δ, and ε, which differ in their symmetry and connectivity between the trimer units. The α isomer has all four trimers connected by corner sharing and has T_d symmetry. Rotating one trimer by 60° reduces the symmetry to C_{3v} in the β isomer, which also has all trimers connected by corners. A second trimer rotation of 60° yields the γ isomer (C_{2v} symmetry), with two trimers corner-linked and two edge-linked. Successive rotation of the third and fourth trimers by 60° results in the δ and ε isomers, respectively. The δ isomer has C_{3v} symmetry with three trimers connected by edges and one linked by corners. All four trimers of the ε isomer are edge-linked with T_d symmetry.

Recently, we added three new sodium-centered butyltin members to the Sn Keggin family: a β isomer (β-$NaSn_{12}$), a γ isomer (γ-$NaSn_{12}$), and a γ isomer capped with an additional Sn (γ-$NaSn_{13}$).[11] Other members of this family include our previously isolated Sn-capped butyltin β isomer (β-$NaSn_{13}$)[12] and the first reported alkyltin Keggin ion, an isopropyltin γ isomer.[7] More recently, Zhu et al. stabilized the γ isomer of the Na-centered butyltin Keggin ion with borate capping, including a bicapped $NaSn_{14}$ structure.[13] The alkyl-Sn Keggin family exhibits differentiating structural features. While a majority of metal cations favor the higher-symmetry α (Nb, W, Mo, and Fe) and ε (Al and Sb) structures, as well as the δ isomer (Cr and Al), we and others have been able to experimentally isolate alkyltin clusters only as the rarer β and γ isomers.[7,11−13] Isomerization between α and β tungstate Keggin ions has been investigated experimentally[14] and computationally.[15] Both conclude that (1) the α isomer is generally favored, and (2) $\alpha \rightarrow \beta$ isomerization is favored with increasing XO_4^{n-} charge on the central tetrahedron (X is the central tetrahedral cation). Meanwhile, the growing alkytin Keggin cluster family is the only one thus far that favors the lowest-symmetry γ isomer. In addition, our previously isolated butyltin Keggin clusters showed evidence of facile interconversion between isomers in solution,[11] complicating characterization by tin, carbon, and proton nuclear magnetic resonance (NMR).

In our previous study, we hypothesized that the charge of the six-coordinate addenda metal may play a role in determining which Keggin isomer would be more favorable.[11]

Received: November 6, 2019
Published: February 14, 2020

https://dx.doi.org/10.1021/acs.inorgchem.9b03261
Inorg. Chem. 2020, 59, 2900−2909

We also investigated the influence of capping for enhancing isomerization.[16] However, it is possible that the size and charge of the central atom of the Keggin ion may also be an important factor in promoting isomerization. Zhang et al. showed computationally that the central cavity for organoantimonate Keggin ions increases in size when going from the α to β isomer.[17] In addition, the central cavity increases in size as the charge of the central tetrahedron $\{MO_4\}$ becomes more positive.[18] It is noteworthy that the Na central cation for our butyltin Keggin clusters has a significantly larger ionic radius and a lower charge (0.99 Å, 1+) than the central cations of the most common Keggin structures, e.g., Si (0.26 Å, 4+) and P (0.17 Å, 5+).[19] To examine the effect of the central cation on the properties of the Keggin ion, we have crystallized a new butyltin β-Keggin ion with Ca at the center {formulated $[(BuSn)_{12}(CaO_4)(OCH_3)_{12}(O)_4(OH)_8]^{2+}$, β-$CaSn_{12}$ henceforth} via a one-step synthesis and studied its solution behavior. Calcium is similar in size to sodium (ionic radius of 1.00 Å),[19] which allows it to fit in the central cavity of the alkyltin Keggin ion. To the best of our knowledge, β-$CaSn_{12}$ is the only Keggin ion that has been isolated having a Ca^{2+} ion in the tetrahedral center. The typical coordination number for Ca is 6−8, and it is rare to find examples of Ca with a coordination number as low as 4.[20] In fact, there is only one molecular compound in the literature containing the T_d $\{CaO_4\}$ unit, and it required the use of very bulky alkoxide ligands to stabilize the Ca^{2+} centers.[21] Here we provide complete solution characterization of β-$CaSn_{12}$ by electrospray ionization mass spectrometry (ESI-MS), multinuclear (^{1}H, ^{13}C, and ^{119}Sn) NMR, and small-angle X-ray scattering (SAXS).

Additionally, we report here room-temperature aging studies in the solution and solid state for the Ca-centered butyltin Keggin cluster and heating studies monitored by variable-temperature NMR. Understanding the long-term stability and solution behavior of these organotin materials is important for applications such as high-resolution nanolithography.[22] These aging and heating studies provided insight into the prior suspected isomerization (or lack thereof) occurring in solution for these alkyl-Sn Keggin clusters. Over time, the methoxy ligands of the clusters (derived by synthesis in methanol) undergo hydrolysis and are replaced with hydroxyl ligands. This was monitored in solution by ^{1}H NMR and in the solid state by Fourier transform infrared spectroscopy (FT-IR). We have also employed density functional theory (DFT) computational studies to compare the relative stabilities of the Ca- and Na-centered clusters.

■ RESULTS AND DISCUSSION

Synthesis. The Na-centered Keggin clusters used for aging studies were synthesized by combining stock solutions of 0.1 M $BuSnCl_3$ in MeOH and 0.1 M NaOH in MeOH at room temperature in a 1:4 ratio, as reported previously.[11] β-$CaSn_{12}$ was synthesized by combining a 0.1 M solution of $BuSnCl_3$ in MeOH with 2 molar equivalents of solid $Ca(OH)_2$ in a Parr reactor that was heated to 100 °C for 24 h. Though the stoichiometry is the same between the two reactions (1 Sn:4 OH), the reactant concentrations are much higher in the β-$CaSn_{12}$ synthesis as $Ca(OH)_2$ is added as a solid rather than a solution. In addition, the solvothermal conditions are necessary to dissolve the $Ca(OH)_2$ and force the calcium into the low-coordination environment at the center of the cluster. The reaction does not proceed at room temperature.

Single-Crystal Structure of β-$CaSn_{12}$. The single-crystal X-ray structure of β-$CaSn_{12}$, fully formulated $[(BuSn)_{12}(CaO_4)(OCH_3)_{12}(O)_4(OH)_8]^{2+}\cdot s2[OH^-]$, is shown in Figure 1 and Figure S1. This compound has the same structure and ligand arrangement as our previously reported β-$NaSn_{12}$ but has Ca at the center instead of Na.[11] Elemental analysis by SEM-EDX was used to confirm the presence of Ca and minimal Na (from Ca) in the crystals of β-$CaSn_{12}$ (Table S2). However, the Na is present as NaCl (minimal Cl also observed), and no Na-centered clusters are observed by ESI-MS (discussed below). Each Sn has a terminal butyl ligand, and the bridging μ_2-oxygens between trimers of the Keggin cluster are either oxo or hydroxyl ligands. The bridging μ_3-oxygens found within each of the four trimers are methoxy ligands that come from the methanol reaction solution. The hydrolysis of these methoxy ligands will be discussed in detail below.

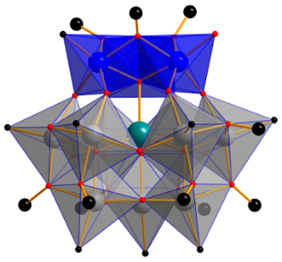

Figure 1. Single-crystal X-ray structure of the β-$CaSn_{12}$ $[(BuSn)_{12}(CaO_4)(OCH_3)_{12}(O)_4(OH)_8]^{2+}$ molecule. Gray and blue polyhedra represent Sn; Ca is colored teal, O red, and C black. Butyl chains have been omitted, with only the Sn-bound carbon shown, for ease of viewing.

β-$CaSn_{12}$ has a charge of 2+ with two hydroxide counterions. The charge was determined on the basis of ESI-MS data and bond valence sum (BVS) calculations (Table S1). Only one OH^- was identified in the crystal lattice, but on the basis of SQUEEZE[23] analysis, there is room in the crystal packing for an additional hydroxide counterion. As is commonly observed for metal−oxo clusters, the BVS values for bridging oxo ligands are ambiguous, with values ranging from 1.16 to 1.41 (average of 1.32), due to disordered protons that cannot be located crystallographically. To be consistent with an overall charge of 2+, oxos with a BVS of ≥1.37 were assigned as O^{2-} and the remaining oxos as OH^-. In addition, the average BVS of 1.32 is in agreement with the $^2/_3$ OH^- and $^1/_3$ O^{2-} to correspond with the 2+ charge observed by ESI-MS (discussed below).

Changing the central cation does have a significant effect on the bond lengths of the four central oxos. For β-$NaSn_{12}$, the average Na−O bond length is 2.32 Å, and for β-$CaSn_{12}$, the average Ca−O bond length is 2.28 Å. The higher charge of Ca^{2+} leads to slightly shorter bonds to the surrounding oxos. Consequently, the Sn−O bonds of the central oxos of β-$CaSn_{12}$ are lengthened. The average Sn−O bond length for the central oxos of β-$CaSn_{12}$ is 2.11 Å, and that for β-$NaSn_{12}$ is 2.08 Å. These values are summarized in Table 1. The BVS of the central Ca is 1.7, while those for the tetrahedral O^{2-} bound to Ca are high (>2.0). Although the BVS for Ca^{2+} is a bit low, this may be due to the fact that the parameters[24] used in the BVS calculations are empirically derived from metal oxide lattices, not molecules. As mentioned previously, the coordination environment of the central Ca is unique and

Table 1. Average Bond Lengths for O Atoms of the Central Tetrahedron

	average Na/Ca−O bond length (Å)	average Sn−central O bond length (Å)
β-NaSn$_{12}$	2.32 (1)	2.08 (1)
β-CaSn$_{12}$	2.28 (2)	2.11 (1)

there are no other structures in the literature that contain tetrahedral calcium within an inorganic framework.

Electrospray Ionization Mass Spectrometry (ESI-MS). ESI-MS of β-CaSn$_{12}$ crystals dissolved in methanol (Figure 2a) shows one main ion species at m/z 1259.85, corresponding to a molecule with a 2+ charge (based on peak-to-peak separations in the peak envelope). Minor peaks are observed at m/z 1282.83 (2+ charged species) and m/z 2557.63 (1+ charged species). The peak envelopes corresponding to species with a 2+ charge were simulated as a combination of eight overlapping peaks, shown in Figure 2b and listed in Table 2. The largest contributor to the overlapping peaks has the formula $[(C_4H_9Sn)_{12}(CaO_4)(O)_{11}(OH)_4(OCH_3)_2]^{2+}$ and comprises 59% of the total peak simulation. Though the intact ion with all ligands present was not detected, all of the assigned peaks have formulas that correspond to species containing 12 butyltin groups, a calcium center, and varying numbers of oxo, hydroxyl, and methoxy ligands. All of the formulas in Table 2 have fewer than the 40 ligands required for the complete cluster, but this is likely due to the fragmentation process. Unfortunately, the intensity of the peak at m/z 2557.63 was too low to accurately assign. No peaks were detected in the negative ionization mode, and importantly, no Na-centered clusters were observed. Full peak assignments can be found in Figures S2−S9.

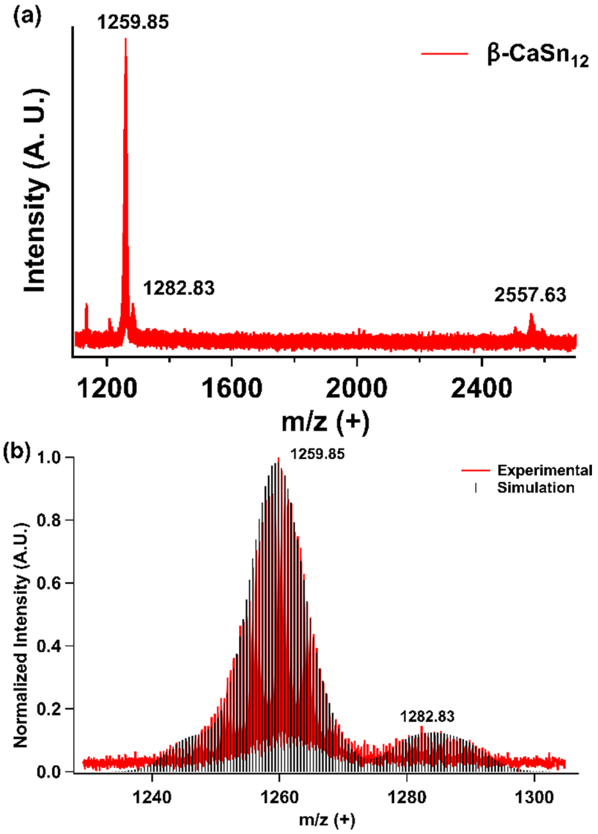

Figure 2. (a) Full ESI-MS spectrum of β-CaSn$_{12}$ in methanol. Positive ionization mode, 100 V fragmentation. (b) Experimental (red) and simulated (black) peak envelopes for main ion species. The simulation is a combination of eight overlapping peaks (see Table 2).

Table 2. ESI-MS Peak Assignments for β-CaSn$_{12}$ in Methanol

formula	observed m/z	calculated m/z	% contribution
$[(C_4H_9Sn)_{12}(CaO_4)(O)_{11}(OH)_6]^{2+}$	1245.83	1245.79	6.7
$[(C_4H_9Sn)_{12}(CaO_4)(O)_{10}(OH)_8]^{2+}$	1254.85	1254.79	13.4
$[(C_4H_9Sn)_{12}(CaO_4)(O)_{11}(OH)_4(OCH_3)_2]^{2+}$	1259.85	1259.80	59.0
$[(C_4H_9Sn)_{12}(CaO_4)(O)_{11}(OH)_3(OCH_3)_3]^{2+}$	1266.85	1266.81	7.4
$[(C_4H_9Sn)_{12}(CaO_4)(O)_8(OH)_{11}(OCH_3)]^{2+}$	1279.84	1279.81	4.0
$[(C_4H_9Sn)_{12}(CaO_4)(O)_{10}(OH)_4(OCH_3)_4]^{2+}$	1282.83	1282.83	3.4
$[(C_4H_9Sn)_{12}(CaO_4)(O)_8(OH)_{10}(OCH_3)_2]^{2+}$	1286.83	1286.82	2.7
$[(C_4H_9Sn)_{12}(CaO_4)(O)_{10}(OH)_3(OCH_3)_5]^{2+}$	1289.81	1289.83	3.4

Nuclear Magnetic Resonance (NMR) Spectroscopy. One of the most important features of CaSn$_{12}$ is that it predominantly forms the β isomer. The Na-centered clusters always crystallize as a mixture of β and γ isomers, and solution state NMR characterization of these compounds suggests that there may be interconversion between isomers, as well.[11] Having mainly one isomer present in solution significantly reduces the difficulty of solution characterization. The ^{1}H and ^{119}Sn NMR spectra for β-CaSn$_{12}$ in C_6D_6 are shown in panels a and b of Figure 3, respectively, and β,γ-NaSn$_{12}$ is also included to highlight the difference in the complexity of NMR spectra when multiple isomers are present versus one. Expanded spectral views and ^{13}C data can be found in Figures S10−S12. The ^{1}H NMR spectrum for β-CaSn$_{12}$ shows much sharper and better-defined peak splitting than does β,γ-NaSn$_{12}$, but the ^{119}Sn NMR is most telling. Due to the mixture of isomers present in β,γ-NaSn$_{12}$ as well as suspected isomerization in solution, there are many different Sn environments present, resulting in several Sn peaks in the six-coordinate region. The ^{119}Sn spectrum of β-CaSn$_{12}$ has just three sharp peaks in the six-coordinate region in a 2:1:1 ratio, consistent with the different Sn environments of the β isomer.

The three Sn sites are shown in Figure 3b, and each peak has been assigned to its respective site on the basis of integration and ^{119}Sn−^{117}Sn coupling constants. Coupling constants were also used to assign peaks in the ^{183}W NMR spectrum of the β-AlW$_{12}$O$_{40}$ Keggin ion.[14] Site 1 (blue) contains the three Sn sites of the 60° rotated trimer at the top of the cluster that defines the molecular C_3 axis; site 2 (green) contains the six Sn sites in the middle "belt", and site 3 (gray) contains the three Sn sites of the trimer opposite to those of site 1. The peak at −469.5 ppm with an integrated value of 2 (normalized to peak 1) corresponds to the six Sn sites in the middle belt of the cluster (site 2). The peak at −471.0 ppm has a coupling constant of 147 Hz and corresponds to site 3, while the peak at −474.6 ppm has a coupling constant of 175 Hz and corresponds to site 1. The larger coupling constant indicates a larger distance between neighboring Sn sites. The Sn−Sn distance between sites 1 and 2 in the crystal structure of β-

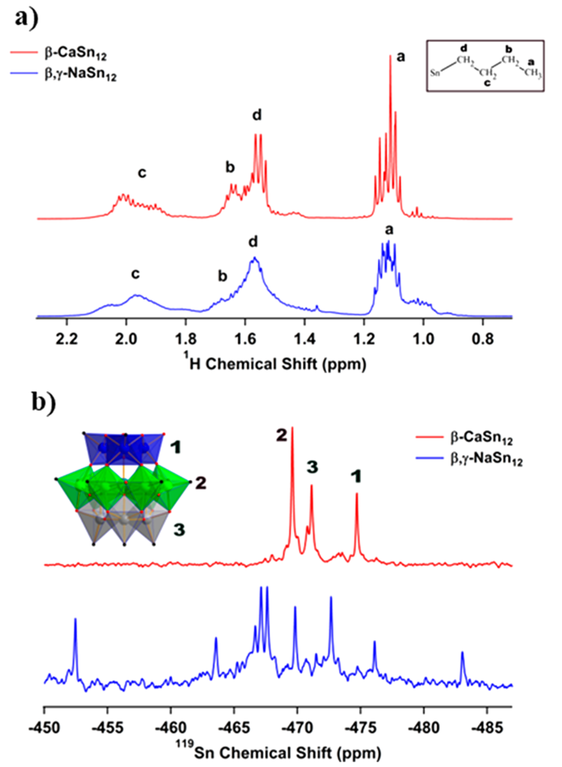

Figure 3. (a) ^{1}H NMR spectrum of β-$CaSn_{12}$ (red) and β,γ-$NaSn_{12}$ (blue) in C_6D_6. (b) ^{119}Sn NMR spectrum of β-$CaSn_{12}$ (red) and β,γ-$NaSn_{12}$ (blue) in C_6D_6. The inset shows a depiction of the three Sn sites of β-$CaSn_{12}$.

$CaSn_{12}$ is 3.8 Å, and the Sn−Sn distance between sites 2 and 3 is 3.4 Å. These values are also summarized in Table 3. The asymmetry of the satellites on peaks 2 and 3 of the ^{119}Sn spectrum of β-$CaSn_{12}$ will be discussed in further detail below. On the other hand, we are unable to assign specific Sn sites for β,γ-$NaSn_{12}$ due to the multitude of peaks, including satellite peaks from ^{119}Sn−^{117}Sn coupling.

Table 3. Coupling Constants, Sn−Sn Distances, and Peak Assignments for ^{119}Sn Peaks of β-$CaSn_{12}$

δ (ppm)	distance between satellites (Hz)	Sn−Sn distance to the middle layer (Å)	assignment
−469.5	165	–	site 2
−471.0	147	3.4	site 3
−474.6	175	3.8	site 1

Small-Angle X-ray Scattering (SAXS). As shown in Figure 4, SAXS of β-$CaSn_{12}$ in tetrahydrofuran (THF) (red) shows a pure and monodisperse solution that is consistent with the simulated scattering curve (black) based on the single-crystal structure. The deviation between the simulated and experimental curves around $q = 0.4$ Å^{-1} is due to a structure factor, or ordering of clusters in solution. This behavior has also been observed with our previously isolated β-$NaSn_{13}$ Keggin cluster.[12] The experimental data were fit with a single-population spherical model that also accounted for the structure factor. The radius determined from this model was 4.92 Å, consistent with the cluster radius determined from the single-crystal structure (5.0 Å). Moreover, the oscillations between q values of 0.9 and 2.5 Å^{-1} are visible, indicating a monospecific solution. The aforementioned structure factor indicates clusters that are ~9 Å apart, which requires some interdigitation of butyl chains (see Figure S13 for model and fitting parameters).

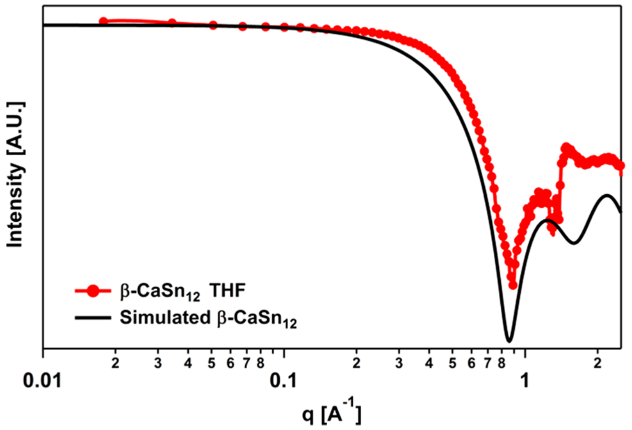

Figure 4. Small-angle X-ray scattering data for β-$CaSn_{12}$ in THF (red) and the simulated scattering curve (black).

Aging Studies. Butyl-Sn Keggin clusters are being considered for potential applications in solution-deposited thin films, so it is important to understand the aging behavior of these clusters both in solution and in the solid state in air. We observed previously that the methoxy ligands of β,γ-$NaSn_{12}$ exhibited hydrolysis in solution.[11] Here we describe the hydrolysis process for β-$CaSn_{12}$ as a function of solvent composition (C_6D_6, $CDCl_3$, 9:1 C_6D_6/CD_3OD, and 9:1 $CDCl_3/CD_3OD$) via ^{1}H NMR. FT-IR tracks the hydrolysis process in air via the intensity of the methoxy C−O stretch absorbance at ~1050 cm^{-1}.

NMR. ^{1}H NMR is a technique commonly used to monitor and quantify the extent of reactions in the solution state[25,26] and is ideal for measuring the hydrolysis of methoxy ligands to hydroxyl ligands. The peaks corresponding to bound methoxy and free methanol protons are clearly visible in the ^{1}H NMR spectrum of β-$CaSn_{12}$. Because methanol is a product of the hydrolysis of methoxy to hydroxyl ligands, the relative integrated areas of the two peaks over time provide information about the reaction rate and how it is affected by different solvents. Figure 5 shows the ^{1}H NMR spectra of β-$CaSn_{12}$ in C_6D_6 and a 9:1 C_6D_6/CD_3OD mixture for fresh solutions (0 days) through day 4 of aging. The analogous spectra recorded in $CDCl_3$ and a 9:1 $CDCl_3/CD_3OD$ mixture are shown in Figure S14. The broad peak at approximately 3.6 ppm corresponds to the bound -OCH_3 protons, and the sharp peak at 3.0−3.2 ppm corresponds to methanol CH_3- protons. These peaks were integrated a total of three times each, and their average relative areas compared for each spectrum (Figure 6).

β-$CaSn_{12}$ exhibits hydrolysis in all of the solvents studied and shows that hydrolysis is slowest in C_6D_6 and fastest in $CDCl_3$. Adding excess deuterated methanol increases the rate of hydrolysis in benzene but does not increase the rate in chloroform. The difference in the rate of hydrolysis in different solvents is most likely due to the amount of residual water present in solution. Due to the proposed application of these clusters, we need to investigate their behavior in non-rigorously controlled environments, so the deuterated solvents were not dried prior to the aging study. They likely contain trace amounts of water, promoting the hydrolysis process.

https://dx.doi.org/10.1021/acs.inorgchem.9b03261
Inorg. Chem. 2020, 59, 2900−2909

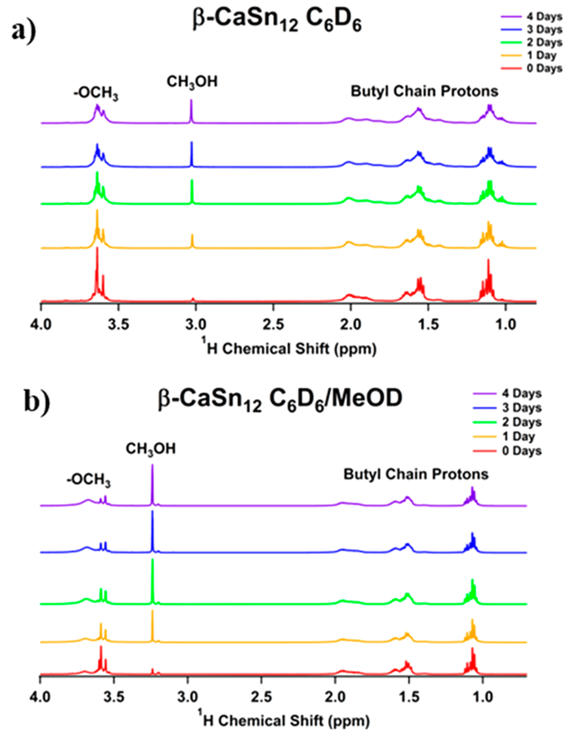

Figure 5. ^{1}H NMR spectra following aging of β-CaSn$_{12}$ in C$_6$D$_6$ and a 9:1 C$_6$D$_6$/MeOD mixture.

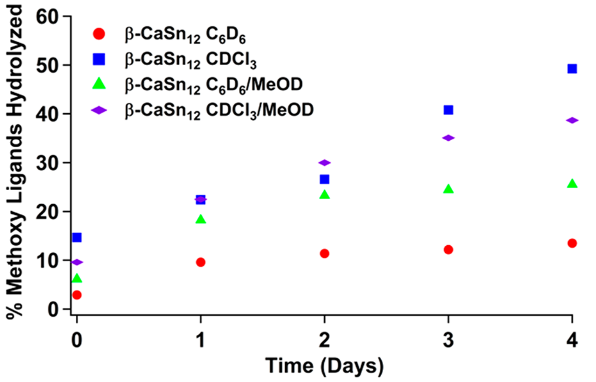

Figure 6. Average percent methoxy ligands hydrolyzed vs the number of days for β-CaSn$_{12}$ in various solvents.

Water is about twice as miscible with chloroform as it is with benzene, consistent with the faster hydrolysis in CDCl$_3$.[27] Adding MeOD to C$_6$D$_6$ likely increases the amount of water in solution, thus increasing the rate of reaction. In the case of the CDCl$_3$/MeOD mixture, it is possible that the MeOD does not add a significant amount of water compared to what was already present in the CDCl$_3$. Unfortunately, it is difficult to quantify the amount of residual water in solution, especially in CDCl$_3$, as the ^{1}H NMR peak corresponding to H$_2$O (~1.56 ppm) overlaps with the butyl ligand protons on the cluster. There is a very small peak at approximately 0.3 ppm in the ^{1}H spectra of β-CaSn$_{12}$ in C$_6$D$_6$ that corresponds to water in solution (Figure S10).

Integrating the peaks of interest is straightforward in benzene where the peaks are well-separated but is more complex in chloroform where the bound and free -OCH$_3$ peaks overlap. As a further complication, the spectra with excess MeOD exhibit a second free methanol resonance slightly upfield of the main methanol peak, potentially due to the formation of CH$_3$OD after exchange of CD$_3$OD with -OCH$_3$ ligands on the cluster. This is not a major concern for the spectra in the C$_6$D$_6$/MeOD mixture but does add another layer of complexity to the integration of overlapping peaks in spectra recorded in a CDCl$_3$/MeOD mixture. Peaks also tend to broaden and overlap as aging progresses in all solvents. Despite these difficulties, the deviation between separate integration measurements is estimated to be between 1% and 8%. Perhaps with the exception of CDCl$_3$, the curves appear to plateau, suggesting an equilibrium is reached between OH$^-$ and OCH$_3^-$/OCD$_3^-$ ligation. The CDCl$_3$ perhaps continues to absorb water with aging, driving the equilibrium forward toward more hydrolysis. However, because equilibrium appears to be reached, even in excess methanol, this suggests neither ligand is favored strongly, and both are labile. However, as noted previously, the methoxy ligand seems necessary for crystallization, as this is the only form we and others have observed with the various butyltin Keggin ions.[11−13]

FT-IR. FT-IR spectra for β-CaSn$_{12}$ were recorded at various time intervals after isolating crystals of the compound from the mother liquor. Spectra were recorded on days 1, 7, 14, 21, and 28. Figure 7 shows an overlay of all of the spectra focused on the C−O stretch of the OCH$_3$ ligand (normalized to the Sn−O absorbance at 530 cm^{-1}). Full spectra are reported in Figure S15. The intensity of the C−O peak for β-CaSn$_{12}$ fluctuates between measurements and does not follow a clear trend. This is consistent with the NMR studies; methanol that is retained in the solid following hydrolysis or from the mother liquor can undergo exchange between OH$^-$ and OCH$_3^-$ ligation.

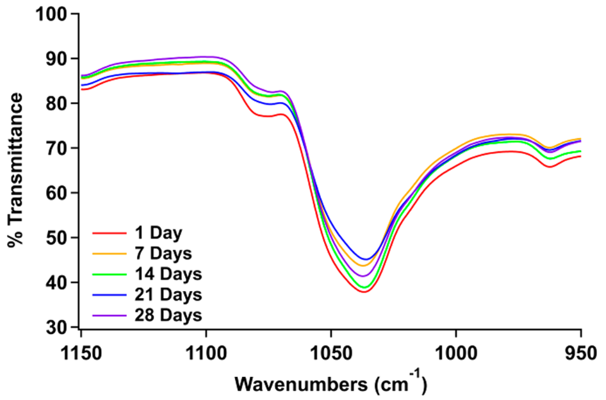

Figure 7. FT-IR spectra showing the change in absorbance of the H$_3$C−O stretch (methoxy ligand) of solid β-CaSn$_{12}$ over time.

In Situ Heating Monitored by NMR. A solution of β-CaSn$_{12}$ in C$_6$D$_6$ was heated in situ and monitored by ^{1}H and ^{119}Sn NMR. Beginning at 30 °C, ^{1}H and ^{119}Sn spectra were recorded (approximately 1 h data collection time) and then the temperature was increased by 10 °C. ^{1}H and ^{119}Sn spectra were recorded at each temperature. Once the temperature reached 60 °C, the temperature was held constant for 3 h. Three ^{119}Sn spectra and four ^{1}H spectra were recorded during this time. Figure 8 shows the resulting spectra from this heating experiment.

The ^{1}H spectra (Figure 8a) do not show much change other than the sharpening of peaks upon heating. Interestingly, the ^{119}Sn spectra show the appearance of new peaks (denoted by arrows in Figure 8b) upon heating, indicating the formation of additional isomers in solution. The peak at −470.7 ppm in the

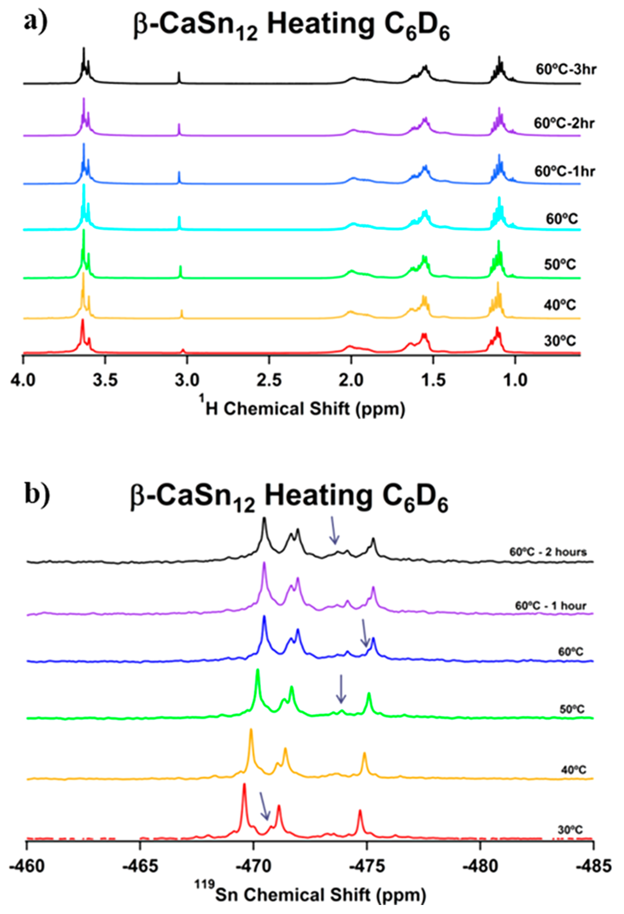

Figure 8. (a) ^{1}H NMR spectra of β-$CaSn_{12}$ in C_6D_6 heated in situ. (b) ^{119}Sn NMR spectra of β-$CaSn_{12}$ in C_6D_6 heated in situ. Gray arrows indicate growth of the γ isomer with heating.

^{119}Sn spectrum was originally thought to be a satellite of the neighboring, more intense peak. However, the intensity of this "satellite" increases with heating, meaning that it is due to the presence of an additional isomer. The presence of this peak at room temperature indicates that the β-$CaSn_{12}$ product is not purely β isomer, but additional isomers are present in only trace amounts. As there are four peaks that increase in intensity due to heating, we hypothesize that these are due to formation of the γ isomer at higher temperatures. When this heated solution is cooled to room temperature, the more complex mixture of isomers is preserved (Figure S16). Initially, this result was puzzling, because the synthesis performed at elevated temperatures yields predominantly the β form. However, there are multiple differences between the synthesis and the NMR experiment described above, including (1) the solvent, (2) excess $Ca(OH)_2$ in the synthesis, and (3) reaction byproducts in the synthesis (i.e., Cl^- from the butyltin trichloride). Despite this isomerization at elevated temperatures, the mixture remains predominantly the β form, illustrating the much slower isomerization of the Ca-centered cluster compared to the Na-centered Keggin.

DFT Computational Analysis. The β and γ isomers of the Na- and Ca-centered Sn Keggin ions were simulated, and their hydrolysis Gibbs free energy and HOMO−LUMO gaps were determined using a thermodynamic cycle in which the hydrolysis energy is the sum of the corresponding gas-phase Gibbs free energy (ΔG_{gas}) and the Gibbs free energies of solvation (ΔG_{solv}; eq 1). The gas-phase term contains a correctional value that takes into account the enthalpy, entropy, and temperature of the system when a frequency analysis is performed. Parametrized continuum solvation models were used to determine the solvation energies, modeling the system in water with a dielectric constant of ~78.36. The thermodynamic cycle for the calcium-centered Keggin isomers is shown in Scheme 1, where n is the coefficient of that species.

Equation 1 is used to determine the hydrolysis Gibbs free energy (ΔG_{aq}) obtained from the thermodynamic cycle shown nin Scheme 1.

$$\Delta G_{aq} = \Delta G_{gas} + \sum_{i=1}^{N\ \text{products}} n_i \Delta G_i^{solv} - \sum_{j=1}^{N\ \text{reactants}} n_j \Delta G_j^{solv} \tag{1}$$

These results are summarized in Table 4 and are in order from most to least stable. We consider clusters to be more stable if they have a relatively low hydrolysis Gibbs free energy and a large HOMO−LUMO gap. To reduce the number of degrees of freedom, methyl was used as the terminal ligand on each tin rather than butyl. Both isomers of $NaSn_{12}$ were assigned the same formula and charge, $[(MeSn)_{12}(NaO_4)(OCH_3)_{12}(O)_4(OH)_8]^+$. Similarly, both isomers of $CaSn_{12}$ were assigned a formula and charge of $[(MeSn)_{12}(CaO_4)$-

Table 4. Calculated Hydrolysis Gibbs Free Energies and HOMO-LUMO Gaps for β and γ Isomers of $NaSn_{12}$ and $CaSn_{12}$

cluster	hydrolysis Gibbs free energy (kcal/mol)	ΔG (kcal/mol) normalized to β-$NaSn_{12}{}^+$	HOMO−LUMO gap (eV)
β-$NaSn_{12}{}^{1+}$	−367.0	0.0	6.21
β-$CaSn_{12}{}^{2+}$	−354.7	12.3	6.23
α-$NaSn_{12}{}^{+}$	−350.5	16.5	6.18
δ-$NaSn_{12}{}^{+}$	−347.1	19.9	6.00
γ-$NaSn_{12}{}^{+}$	−344.8	22.2	5.67
α-$CaSn_{12}{}^{2+}$	−342.8	24.2	6.20
γ-$CaSn_{12}{}^{2+}$	−338.6	28.4	5.73
δ-$CaSn_{12}{}^{2+}$	−338.3	28.7	6.01
ε-$NaSn_{12}{}^{+}$	−306.9	60.1	5.70
ε-$CaSn_{12}{}^{2+}$	−297.2	69.8	5.81

Scheme 1. Thermodynamic Cycle for All Isomers of $CaSn_{12}$

$$12\,Sn(H_2O)_6{}^{4+}{}_{(aq)} + Ca(H_2O)_6{}^{2+}{}_{(aq)} + 3\,CO_{2(aq)} + 21\,CH_{4(aq)} \xrightarrow{\Delta G_{aq}} 48\,H_3O^+_{(aq)} + 8\,H_2O_{(aq)} + C_{24}H_{80}CaO_{28}Sn_{12}{}^{2+}{}_{(aq)}$$

$$\downarrow -\Delta G^{solv}_{Sn(H_2O)_6^{4+}} \quad \downarrow -\Delta G^{solv}_{Ca(H_2O)_6^{2+}} \quad \downarrow -\Delta G^{solv}_{CO_2} \quad \downarrow -\Delta G^{solv}_{CH_4} \qquad \uparrow \Delta G^{solv}_{H_3O^+} \quad \uparrow \Delta G^{solv}_{H_2O} \quad \uparrow \Delta G^{solv}_{C_{24}H_{80}CaO_{28}Sn_{12}^{2+}}$$

$$12\,Sn(H_2O)_6{}^{4+}{}_{(g)} + Ca(H_2O)_6{}^{2+}{}_{(g)} + 3\,CO_{2(g)} + 21\,CH_{4(g)} \xrightarrow{\Delta G_{gas}} 48\,H_3O^+_{(g)} + 8\,H_2O_{(g)} + C_{24}H_{80}CaO_{28}Sn_{12}{}^{2+}{}_{(g)}$$

https://dx.doi.org/10.1021/acs.inorgchem.9b03261
Inorg. Chem. 2020, 59, 2900−2909

$(OCH_3)_{12}(O)_4(OH)_8]^{2+}$. These formulas are consistent with the single-crystal structures and species detected by ESI-MS.

On the basis of DFT calculations, the Na-centered clusters are more stable than their corresponding Ca-centered analogues, likely due to the fact that Na more easily adopts tetrahedral coordination than Ca. Additionally, the extra positive charge of the Ca analogue generally decreases the stability. Importantly, the stability of the β Keggin ion is highest for both Na- and Ca-centered clusters, in agreement with experiment. In addition to having lower symmetry, the γ isomer has two edge-sharing trimers with a shorter metal−metal distance between the two Sn centers that decreases the overall stability of the cluster. The difference in hydrolysis Gibbs free energy between the β and γ isomers for $NaSn_{12}$ is 22.2 kcal/mol, and that for $CaSn_{12}$ is 16.1 kcal/mol, suggesting that $CaSn_{12}$ may isomerize more readily than $NaSn_{12}$. However, we observe the opposite to be true in our experimental studies. We hypothesize that this difference may be attributed to kinetic factors related to the interconversion between isomers. A hydrolysis Gibbs free energy difference of >10 meV/atom is required to confidently state that one isomer is more stable than another.[17,28−31] Because these clusters each have 145 atoms, an energy difference of >34 kcal/mol signals a definitive preference of one isomer over another. The computational stability ordering of the isomers differs slightly from what we observe experimentally, but the differences in hydrolysis Gibbs free energies are below the 34 kcal/mol threshold. Therefore, we can state with certainty only that the β isomers for both systems are more stable than the ε analogues. Returning to the isomerization studies of the classic POM Keggin ions,[14,15] we find isomerization is more favorable with an increasing XO_4^{n-} charge. Consistent with this, we observe greater isomerization behavior in the $\{NaO_4\}^{7-}$-centered cluster than in the $\{CaO_4\}^{6-}$-centered cluster. Another way to view this is the weaker, longer Na−O bond compared to the Ca−O bond permits better lability of the molecule.

CONCLUSION

In summary, we have encapsulated Ca^{2+} into the central tetrahedral cavity of a butyltin β Keggin ion. This is the only member of the growing family of alkyltin Keggin clusters with a central cation other than Na^+. In addition, β-$CaSn_{12}$ provides the first example of four-coordinate Ca^{2+} in an inorganic structure. While alkyltin clusters have been investigated for use in nanolithography, the central Na^+ in the Keggin clusters has raised concern about contamination of expensive lithography fabrication facilities. This study shows that other metal substitutions are possible, which may be later exploited in the functionality of tin oxide materials. Solution characterization by ESI-MS, SAXS, and multinuclear NMR shows that β-$CaSn_{12}$ is free of impurities and contains only trace amounts of other isomers. In comparison to the analogous $NaSn_{12}$ Keggin clusters that always present as mixtures of γ and β isomers, $CaSn_{12}$ is robustly dominated by the β isomer, and it must be heated in solution to drive conversion to a different isomer, presumably γ. This is consistent with the tungstate Keggin ions, in that the lower-charge central cation promotes $\alpha \rightarrow \beta$ isomerization more readily. In this study, the Na-centered cluster seems to establish an equilibrium between isomers at room temperature while the Ca-centered cluster does not isomerize until heat is applied. DFT computations also show a difference in cluster stability with a change in the central cation. Overall, the size and charge of the central cation have a significant effect on the stability and isomerization of the Sn Keggin cluster as a whole. These experimental and computational studies provide additional fundamental insight into the factors that influence Keggin formation and isomer stability.

MATERIALS AND METHODS

All reagents and solvents were purchased from commercial suppliers and used without further purification.

Synthesis of β-$CaSn_{12}$. In a Parr reactor, 15 mL of a 0.1 M stock solution of *n*-$BuSnCl_3$ (95%, 1.5 mmol) in methanol was combined with 0.22 g of solid $Ca(OH)_2$ (3.0 mmol, 4 equiv of OH per Sn), which did not fully dissolve, yielding a cloudy suspension. The suspension was heated solvothermally at 100 °C for 24 h (heating from room temperature to 100 °C occurred over 30 min). The reactor was cooled to room temperature in ∼1 h. Colorless needle crystals were harvested from the walls of the reaction vessel. The yield was approximately 200 mg (45%).

Computational Methods. The computational results were obtained using Gaussian 09.[32] The geometry of each cluster was first optimized in the gas phase using the B3LYP functional.[33] The 6-31G(d) basis set was used for elements Na, Ca, C, H, and O, while the LANL2DZ basis set was used for Sn.[34,35] A frequency calculation was performed to guarantee that there were no imaginary vibration modes confirming that the system was in a stable/metastable state. The LANL2DZ effective core potential was used for Sn. The geometry was further optimized in water using the SMD continuum solvation model and a solvent accessible surface (SAS).[30] The electronic energy was refined using the B3LYP single point with the 6-311+G(d,p) basis set for elements Na, Ca, C, H, and O and the LANL2DZ basis set for Sn.[36] The solvation energy was found using the B3LYP/6-31G(d) single point with SMD in water and a solvent-excluding surface (with a minimum radius for added spheres of 0.20 and an overlap index of 0.89).

Characterization Techniques. *Small-Angle X-ray Scattering (SAXS).* X-ray scattering data were collected on an Anton Paar SAXSess instrument using Cu Kα radiation (1.54 Å) and line collimation. The instrument was equipped with a two-dimensional image plate for data collection in the q = 0.018−2.5 $Å^{-1}$ range. The lower q resolution is limited by the beam attenuator. Approximately 20 mM solutions were measured in 1.5 mm glass capillaries (Hampton Research). Scattering data of the neat solvent were collected for background subtraction. Scattering was measured for 30 min for every experiment. We used SAXSQUANT software for data collection and treatment (normalization, primary beam removal, background subtraction, desmearing, and smoothing to remove the extra noise created by the desmearing routine). All analyses and curve fitting to determine the R_g, size, shape, and size distribution were carried out utilizing IRENA macros with IgorPro 6.3 (Wavemetrics) software.[37] To simulate scattering data from the crystal structure, we used SolX software.[38]

Nuclear Magnetic Resonance Spectroscopy (NMR). ^1H, ^{13}C, and ^{119}Sn NMR spectra were recorded on a Bruker Ascend spectrometer (500 MHz for ^1H, 125 MHz for ^{13}C, and 186 MHz for ^{119}Sn) with a 5 mm BBO probe at 30.0 °C. Chemical shifts are reported in parts per million (δ), and ^1H and ^{13}C spectra are referenced to C_6D_6 and $CDCl_3$ solvent signals.[39] ^{119}Sn NMR is referenced to $SnCl_4$ in C_6D_6.

Electrospray Ionization Mass Spectrometry (ESI-MS). ESI-MS was carried out using an Agilent 6230 ESI-MS system comprised of a time-of-flight (TOF) mass spectrometer coupled to an electrospray ionizer. The crystallized Keggin product, β-$CaSn_{12}$ (1.2 mM Sn), was dissolved in methanol and infused into the ESI-MS system at a flow rate of 0.4 mL min^{-1} using a syringe pump. The solutions were nebulized with the aid of heated N_2 (325 °C) flowing at 8 L min^{-1} and a pressure of 35 psig (241 kPa). The voltages of the capillary, skimmer, and RT octopole were set at 3500, 65, and 750 V, respectively, while the voltage of the fragmenter was set at 100 V. The data were collected in the positive ionization mode. No ion species were detected in the negative ionization mode.

Single-Crystal X-ray Diffraction Data Collection Analysis. X-ray diffraction intensities for β-$CaSn_{12}$ (CCDC-1949774) were collected at 173 K on a Bruker Apex2 CCD diffractometer using Cu Kα radiation (1.54178 Å). Space groups were determined on the basis of systematic absences. Absorption corrections were applied by SADABS,[40] and additional absorption correction was based on the real (μr) value of the crystal used for data collection. The structure was determined by direct methods and Fourier techniques and refined on F^2 using full matrix least-squares procedures. All non-H atoms were refined with anisotropic thermal parameters. All H atoms were refined in calculated positions in a rigid group model. H atoms in bridge -OH groups and in counterions were not found and not taken into consideration. The molecule is located in the crystal structure on a mirror plane. The found structure has a low resolution. The terminal *t*-Bu groups in the structure are significantly disordered, and X-ray diffraction at large angles from crystals of this compoundis was very weak. Even using a strong Incoatec IμS Cu source, reflections with $I/\sigma(I)$ of >1 were only up to $2\theta_{max} = 100°$. Only these reflections were used in the final refinement. Regardless, it provides the appropriate number of reflections per refined parameters, 5031/509. The terminal *t*-Bu groups are highly disordered, and their thermal ellipsoids are significantly elongated. One of these groups was refined as disordered over two positions related by a mirror plane. All terminal groups were refined with restrictions on its geometry; the standard interatomic distances were used as targets for the corresponding contacts. Some short H···H contacts in the structure do not correspond to real contacts between the H atoms but are rrelated to the fact that these groups were refined as a solid unit and its disorder was not resolved. Significant elongation for the C atoms in the butyl ligads and a large maximum shift for its thermal parameters indicate that the disorder of terminal groups in the structure seems to be more complex. In addition, one of the two OH^- counterions in the structure is disordered over two positions related by an inversion center. We could not find a position of the second OH^- counterion needed to provide charge balance. Checking the structure by SQUEEZE[23] indicated there is an additional empty space suitable for the second OH^- counterion. Convergence of the final refinement was not optimal due to the presence of many highly disordered groups in the structure. The RIGU option was used for the final refinement of the structure.

This structure typifies cluster structures with a well-defined central core and highly disordered terminal groups forming an external shell to the structure. X-ray diffraction from such structures is well-defined at small angles and drops to zero at large angles. We made several attempts to obtain a better quality X-ray structure for β-$CaSn_{12}$. Diffraction data have been collected with crystals of different sizes, using both Mo and Cu radiation. In all cases, diffraction intensities with $I > 2\sigma(I)$ were found only up to a resolution of 1.36 Å, and reflections having ratio $I/\sigma(I) > 2$ were found only up to a resolution of 1.15 Å. Data collections at 100 K (with both Mo and Cu sources) did not improve intensity statistics. The structure has been checked in possible monoclinic systems with angles close to 90°. All of these efforts did not improve the X-ray structure for this compound. Although the found structure has a low resolution, it is given in the paper because the framework of the structure is clear, consistent with other characterization, and confirms the main chemical results discussed in this work. All calculations were performed with the Bruker SHELXL package.[41]

Crystallographic Data for β-$CaSn_{12}$. $C_{60}H_{154}CaO_{29}Sn_{12}$, M = 2804.18, 0.11 mm × 0.06 mm × 0.03 mm, T = 173 K, orthorhombic, space group *Pbcm*, a = 16.1505(6) Å, b = 24.9896(11) Å, c = 23.5117(11) Å, V = 9489.2(7) Å^3, Z = 4, D_c = 1.963 Mg/m^3, μ(Cu) = 25.663 mm^{-1}, $F(000)$ = 5464, $2\theta_{max}$ = 100.0°, 20969 reflections, 5031 independent reflections (R_{int} = 0.1002), R1 = 0.0856, wR2 = 0.2263, and GOF = 1.042 for 5031 reflections (509 parameters) with $I > 2\sigma(I)$, R1 = 0.1455, wR2 = 0.2640, and GOF = 1.051 for all reflections, max/min residual electron density +0.885/−0.648 e Å^{-3}.

Fourier Transform Infrared Spectroscopy (FT-IR). Spectra were recorded on a Nicolet iS10 FT-IR spectrometer with a secondary Nicolet iZ 10 module purchased from Thermo Fisher Scientific Inc. The instrument was equipped with a diamond plate for attenuated total reflectance (ATR) measurements. Spectra were recorded in air.

Scanning Electron Microscopy (SEM) and Energy-Dispersive X-ray Spectroscopy (EDS). Electron micrographs and atomic ratios (%) of the crystalline materials were obtained from a Quanta 600F instrument (FEI) combining a scanning electron microscope and an energy-dispersive X-ray spectrometer.

■ ASSOCIATED CONTENT

Supporting Information

The Supporting Information is available free of charge at https://pubs.acs.org/doi/10.1021/acs.inorgchem.9b03261.

> Bond valence sum calculations for β-$CaSn_{12}$, atomic percentages of β-$CaSn_{12}$ determined by SEM-EDX, complete ESI-MS peak assignments, expanded ^{1}H, ^{13}C, and ^{119}Sn NMR spectra, model of SAXS data, and expanded FT-IR spectra (PDF)

Accession Codes

CCDC 1949774 contains the supplementary crystallographic data for this paper. These data can be obtained free of charge via www.ccdc.cam.ac.uk/data_request/cif, or by emailing data_request@ccdc.cam.ac.uk, or by contacting The Cambridge Crystallographic Data Centre, 12 Union Road, Cambridge CB2 1EZ, UK; fax: +44 1223 336033.

■ AUTHOR INFORMATION

Corresponding Author

May Nyman − *Department of Chemistry, Oregon State University, Corvallis, Oregon 97331, United States;* orcid.org/0000-0002-1787-0518; Email: may.nyman@oregonstate.edu

Authors

Danielle C. Hutchison − *Department of Chemistry, Oregon State University, Corvallis, Oregon 97331, United States*
Rebecca D. Stern − *Department of Materials Science and Engineering, University of California, Berkeley, Berkeley, California 94720, United States*
Lev N. Zakharov − *Department of Chemistry, Oregon State University, Corvallis, Oregon 97331, United States*
Kristin A. Persson − *Department of Materials Science and Engineering, University of California, Berkeley, Berkeley, California 94720, United States; Lawrence Berkeley National Laboratory, Berkeley, California 94720, United States;* orcid.org/0000-0003-2495-5509

Complete contact information is available at: https://pubs.acs.org/10.1021/acs.inorgchem.9b03261

Notes

The authors declare no competing financial interest.

■ ACKNOWLEDGMENTS

This work was funded by the National Science Foundation, Center for Chemical Innovation, Grant CHE-1606982. The authors also acknowledge the support of the Oregon State University NMR Facility funded in part by the National Institutes of Health, HEI Grant 1S10OD018518, and by M. J. Murdock Charitable Trust Grant 2014162.

■ REFERENCES

(1) Keggin, J. F. The structure and formula of 12-phosphotungstic acid. *Proc. R. Soc. London, Ser. A* **1934**, *144* (851), 75−100.

(2) Nyman, M.; Bonhomme, F.; Alam, T. M.; Rodriguez, M. A.; Cherry, B. R.; Krumhansl, J. L.; Nenoff, T. M.; Sattler, A. M. A General Synthetic Procedure for Heteropolyniobates. *Science* **2002**, *297* (5583), 996−998.

(3) Sadeghi, O.; Zakharov, L. N.; Nyman, M. Aqueous formation and manipulation of the iron-oxo Keggin ion. *Science* **2015**, *347* (6228), 1359−1362.

(4) Johansson, G.; Gullman, L.-O.; Kjekshus, A.; Söderquist, R. On the Crystal Structure of Some Basic Aluminium Salts. *Acta Chem. Scand.* **1960**, *14*, 771−773.

(5) Wang, W.; Fullmer, L. B.; Bandeira, N. A. G.; Goberna-Ferrón, S.; Zakharov, L. N.; Bo, C.; Keszler, D. A.; Nyman, M. Crystallizing Elusive Chromium Polycations. *Chem.* **2016**, *1* (6), 887−901.

(6) Baskar, V.; Shanmugam, M.; Helliwell, M.; Teat, S. J.; Winpenny, R. E. P. Reverse-Keggin Ions: Polycondensation of Antimonate Ligands Give Inorganic Cryptand. *J. Am. Chem. Soc.* **2007**, *129* (11), 3042−3043.

(7) Reuter, H. Inclusion of Metal Ions within a Tin—Oxygen Cage Stabilized by Organic Residues: Crystal Structure of $[(^{i}PrSn)_{12}O_4(OH)_{24}][Ag_7I_{11}] \cdot NaCl \cdot H_2O \cdot 10DMSO$. *Angew. Chem., Int. Ed. Engl.* **1991**, *30* (11), 1482−1484.

(8) Wang, W.; Amiri, M.; Kozma, K.; Lu, J.; Zakharov, L. N.; Nyman, M. Reaction Pathway to the Only Open-Shell Transition-Metal Keggin Ion without Organic Ligation. *Eur. J. Inorg. Chem.* **2018**, *2018* (42), 4638−4642.

(9) Sadeghi, O.; Falaise, C.; Molina, P. I.; Hufschmid, R.; Campana, C. F.; Noll, B. C.; Browning, N. D.; Nyman, M. Chemical Stabilization and Electrochemical Destabilization of the Iron Keggin Ion in Water. *Inorg. Chem.* **2016**, *55* (21), 11078−11088.

(10) Baker, L. C. W.; Figgis, J. S. New fundamental type of inorganic complex: hybrid between heteropoly and conventional coordination complexes. Possibilities for geometrical isomerisms in 11-, 12-, 17-, and 18-heteropoly derivatives. *J. Am. Chem. Soc.* **1970**, *92* (12), 3794−3797.

(11) Hutchison, D. C.; Stern, R. D.; Olsen, M. R.; Zakharov, L. N.; Persson, K. A.; Nyman, M. Alkyltin clusters: the less symmetric Keggin isomers. *Dalton Trans.* **2018**, *47* (29), 9804−9813.

(12) Saha, S.; Park, D.-H.; Hutchison, D. C.; Olsen, M. R.; Zakharov, L. N.; Marsh, D.; Goberna-Ferrón, S.; Frederick, R. T.; Diulus, J. T.; Kenane, N.; Herman, G. S.; Johnson, D. W.; Keszler, D. A.; Nyman, M. Alkyltin Keggin Clusters Templated by Sodium. *Angew. Chem., Int. Ed.* **2017**, *56* (34), 10140−10144.

(13) Zhu, Y.; Olsen, M. R.; Nyman, M.; Zhang, L.; Zhang, J. Stabilizing γ-Alkyltin-Oxo Keggin Ions by Borate Functionalization. *Inorg. Chem.* **2019**, *58* (7), 4534−4539.

(14) Weinstock, I. A.; Cowan, J. J.; Barbuzzi, E. M. G.; Zeng, H.; Hill, C. L. Equilibria between α and β Isomers of Keggin Heteropolytungstates. *J. Am. Chem. Soc.* **1999**, *121* (19), 4608−4617.

(15) López, X.; Maestre, J. M.; Bo, C.; Poblet, J.-M. Electronic Properties of Polyoxometalates: A DFT Study of α/β-$[XM_{12}O_{40}]^{n-}$Relative Stability (M = W, Mo and X a Main Group Element). *J. Am. Chem. Soc.* **2001**, *123* (39), 9571−9576.

(16) Stern, R. D.; Hutchison, D. C.; Olsen, M. R.; Zakharov, L. N.; Nyman, M.; Persson, K. A. Alkyltin Keggin clusters as EUVL photoresist technology. In *International Conference on Extreme Ultraviolet Lithography 2019*; International Society for Optics and Photonics, 2019; Vol. *11147*, p 111471L.

(17) Zhang, F.-Q.; Guan, W.; Zhang, Y.-T.; Xu, M.-T.; Li, J.; Su, Z.-M. On the Origin of the Inverted Stability Order of the Reverse-Keggin $[(MnO_4)(CH_3)_{12}Sb_{12}O_{24}]^{6-}$: A DFT Study of α, β, γ, δ, and ε Isomers. *Inorg. Chem.* **2010**, *49* (12), 5472−5481.

(18) Zhang, F.-Q.; Zhang, X.-M.; Wu, H.-S.; Jiao, H. Structural and Electronic Properties of Hetero-Transition-Metal Keggin Anions: A DFT Study of α/β-$[XW_{12}O_{40}]^{n-}$(X = Cr^{VI}, V^{V}, Ti^{IV}, Fe^{III}, Co^{III}, Ni^{III}, Co^{II}, and Zn^{II}) Relative Stability. *J. Phys. Chem. A* **2007**, *111* (1), 159−166.

(19) Shannon, R. D. Revised Effective Ionic Radii and Systematic Studies of Interatomic Distances in Halides and Chalcogenides. *Acta Crystallogr., Sect. A: Cryst. Phys., Diffr., Theor. Gen. Crystallogr.* **1976**, *32* (5), 751−767.

(20) Katz, A. K.; Glusker, J. P.; Beebe, S. A.; Bock, C. W. Calcium Ion Coordination: A Comparison with That of Beryllium, Magnesium, and Zinc. *J. Am. Chem. Soc.* **1996**, *118* (24), 5752−5763.

(21) Tesh, K. F.; Hanusa, T. P.; Huffman, J. C.; Huffman, C. J. Structural relationships between mono- and dimeric bis(alkoxides) and bis(aryloxides) of calcium and barium. X-ray crystal structures of $M(OC_6H_2\text{-t-Bu}_2\text{-2,6-Me-4})_2(THF)_3 \cdot (THF)$ (M = calcium, barium) and $[Ca(\mu\text{-}OR)(OR)(THF)]_2 \cdot 2(toluene)$ [R = C-$(C_6H_5)_2CH_2C_6H_4Cl$-4]. *Inorg. Chem.* **1992**, *31* (26), 5572−5579.

(22) Cardineau, B.; Del Re, R.; Marnell, M.; Al-Mashat, H.; Vockenhuber, M.; Ekinci, Y.; Sarma, C.; Freedman, D. A.; Brainard, R. L. Photolithographic properties of tin-oxo clusters using extreme ultraviolet light (13.5 nm). *Microelectron. Eng.* **2014**, *127*, 44−50.

(23) Van der Sluis, P.; Spek, A. L. BYPASS: an effective method for the refinement of crystal structures containing disordered solvent regions. *Acta Crystallogr., Sect. A: Found. Crystallogr.* **1990**, *46* (3), 194−201.

(24) Brown, I. D.; Altermatt, D. Bond-valence parameters obtained from a systematic analysis of the Inorganic Crystal Structure Database. *Acta Crystallogr., Sect. B: Struct. Sci.* **1985**, *41* (4), 244−247.

(25) Oliveri, A. F.; Colla, C. A.; Perkins, C. K.; Akhavantabib, N.; Callahan, J. R.; Pilgrim, C. D.; Smart, S. E.; Cheong, P. H.-Y.; Pan, L.; Casey, W. H. Isomerization of Keggin Al$_{13}$ Ions Followed by Diffusion Rates. *Chem. - Eur. J.* **2016**, *22* (52), 18682−18685.

(26) Brochier Salon, M.-C.; Bayle, P.-A.; Abdelmouleh, M.; Boufi, S.; Belgacem, M. N. Kinetics of hydrolysis and self condensation reactions of silanes by NMR spectroscopy. *Colloids Surf., A* **2008**, *312* (2), 83−91.

(27) Clifford, C. W. The Solubility of Water in Gasoline and in Certain Other Organic Liquids, Determined by the Calcium Chloride Method. *J. Ind. Eng. Chem.* **1921**, *13* (7), 631−632.

(28) López, X.; Poblet, J. M. DFT Study on the Five Isomers of PW12O403-: Relative Stabilization upon Reduction. *Inorg. Chem.* **2004**, *43* (22), 6863−6865.

(29) André Ohlin, C.; Rustad, J. R.; Casey, W. H. The energetics of isomerisation in Keggin-series aluminate cations. *Dalton Trans.* **2014**, *43* (39), 14533−14536.

(30) Marenich, A. V.; Cramer, C. J.; Truhlar, D. G. Universal solvation model based on solute electron density and on a continuum model of the solvent defined by the bulk dielectric constant and atomic surface tensions. *J. Phys. Chem. B* **2009**, *113* (18), 6378−6396.

(31) Clavería-Cádiz, F.; Arratia-Pérez, R.; MacLeod-Carey, D. Density functional study on Keggin heteropolyanions containing fifth period main group heteroatoms. *Polyhedron* **2016**, *117*, 478−486.

(32) Frisch, M. J.; Trucks, G. W.; Schlegel, H. B.; Scuseria, G. E.; Robb, M. A.; Cheeseman, J. R.; Scalmani, G.; Barone, V.; Petersson, G. A.; Nakatsuji, H.; Li, X.; Caricato, M.; Marenich, A. V.; Bloino, J.; Janesko, B. G.; Gomperts, R.; Mennucci, B.; Hratchian, H. P.; Ortiz, J. V.; Izmaylov, A. F.; Sonnenberg, J. L.; Williams-Young, F.; Ding, F.; Lipparini, F.; Egidi, F.; Goings, J.; Peng, B.; Petrone, A.; Henderson, T.; Ranasinghe, D.; Zakrzewski, V. G.; Gao, J.; Rega, N.; Zheng, G.; Liang, W.; Hada, M.; Ehara, M.; Toyota, K.; Fukuda, R.; Hasegawa, J.; Ishida, M.; Nakajima, T.; Honda, Y.; Kitao, O.; Nakai, H.; Vreven, T.; Throssell, K.; Montgomery, J. A., Jr.; Peralta, J. E.; Ogliaro, F.; Bearpark, M. J.; Heyd, J. J.; Brothers, E. N.; Kudin, K. N.; Staroverov, V. N.; Keith, T. A.; Kobayashi, R.; Normand, J.; Raghavachari, K.; Rendell, A. P.; Burant, J. C.; Iyengar, S. S.; Tomasi, J.; Cossi, M.; Millam, J. M.; Klene, M.; Adamo, C.; Cammi, R.; Ochterski, J. W.; Martin, R. L.; Morokuma, K.; Farkas, O.; Foresman, J. B.; Fox, D. J. *Gaussian 09*; Gaussian, Inc.: Wallingford, CT, 2013.

(33) Becke, A. D. Density-functional thermochemistry. III. The role of exact exchange. *J. Chem. Phys.* **1993**, *98* (7), 5648−5652.

(34) Hariharan, P. C.; Pople, J. A. The influence of polarization functions on molecular orbital hydrogenation energies. *Theoret. Chim. Acta* **1973**, *28* (3), 213−222.

(35) Wadt, W. R.; Hay, P. J. Ab initio effective core potentials for molecular calculations. Potentials for main group elements Na to Bi. *J. Chem. Phys.* **1985**, *82* (1), 284−298.

(36) Krishnan, R.; Binkley, J. S.; Seeger, R.; Pople, J. A. Self-consistent molecular orbital methods. XX. A basis set for correlated wave functions. *J. Chem. Phys.* **1980**, *72* (1), 650−654.

(37) Ilavsky, J.; Jemian, P. R. ıt Irena: tool suite for modeling and analysis of small-angle scattering. *J. Appl. Crystallogr.* **2009**, *42* (2), 347−353.

(38) Zuo, X.; Cui, G.; Merz, K. M.; Zhang, L.; Lewis, F. D.; Tiede, D. M. X-ray diffraction "fingerprinting" of DNA structure in solution for quantitative evaluation of molecular dynamics simulation. *Proc. Natl. Acad. Sci. U. S. A.* **2006**, *103* (10), 3534−3539.

(39) Gottlieb, H. E.; Kotlyar, V.; Nudelman, A. NMR Chemical Shifts of Common Laboratory Solvents as Trace Impurities. *J. Org. Chem.* **1997**, *62* (21), 7512−7515.

(40) Sheldrick, G. M. *SADABS. Siemens Area Detector Absorption Correction Program*, version 2.01; Bruker, 1998.

(41) Sheldrick, G. M. Crystal structure refinement with ıt SHELXL. *Acta Crystallogr., Sect. C: Struct. Chem.* **2015**, *71* (1), 3−8.